Assessing the influence of chemico-osmosis on solute transport in bentonite membranes based on combined phenomenological and physical modeling

Michael Malusis [i)], Andrea Dominijanni [ii)], Joseph Scalia [iii)], Nicolò Guarena [iv)], Kristin Sample-Lord [v)], Gretchen Bohnhoff [vi)], Charles Shackelford [vii)] and Mario Manassero [viii)]

i) Professor, Department of Civil & Environmental Engineering, Bucknell University, Lewisburg, PA, USA.
ii) Associate Professor, Department of Structural, Geotechnical & Building Engineering, Politecnico di Torino, Italy.
iii) Assistant Professor, Department of Civil & Environmental Engineering, Colorado State University, Fort Collins, CO, USA.
iv) Ph.D. Student, Department of Structural, Geotechnical & Building Engineering, Politecnico di Torino, Italy.
v) Assistant Professor, Department of Civil & Environmental Engineering, Villanova University, Villanova, PA, USA.
vi) Associate Professor, Department of Civil & Environmental Engineering, University of Wisconsin-Platteville, Platteville, WI, USA.
vii) Professor, Department of Civil & Environmental Engineering, Colorado State University, Fort Collins, CO, USA.
viii) Professor, Department of Structural, Geotechnical & Building Engineering, Politecnico di Torino, Italy.

ABSTRACT

The ability of bentonite-based barriers to act as semipermeable membranes that inhibit the passage of solutes (ions) is well documented. This behavior induces chemico-osmotic liquid flux that can improve the performance of such barriers by reducing solute mass flux. This paper explores the potential significance of chemico-osmosis on solute transport through bentonite membranes using a phenomenological transport framework combined with a physical model relating the macroscale transport properties (membrane efficiency coefficient, ω, and hydraulic conductivity, k_h) to the microscale physicochemical and fabric properties of the bentonite. The model was used to simulate the coupled transport of monovalent salt (KCl) through a geosynthetic clay liner. The results indicate that the influence of chemico-osmosis is dependent upon the void ratio of the bentonite and the extent to which clay platelets are aggregated to form tactoids. Chemico-osmosis is predicted to have an increasingly more significant impact on solute transport with increasing source concentration (C_{s0}), despite decreasing ω with increasing C_{s0}.

Keywords: bentonite, chemical transport, chemico-osmosis, fabric, geosynthetic clay liner, semipermeable membrane

1 INTRODUCTION

Experimental studies conducted over the past two decades have shown that engineered barriers comprising bentonite clay, such as geosynthetic clay liners (GCLs), can behave as a semipermeable membrane in electrolyte solutions, resulting in restricted solute (ion) migration and, therefore, improved chemical containment (Malusis and Shackelford, 2002a,b; Mazzieri et al., 2003, 2005; Kang and Shackelford, 2011; Bohnhoff and Shackelford, 2013; Dominijanni et al., 2013; Malusis and Daniyarov, 2016; Shackelford et al., 2016; Shackelford and Scalia, 2016; Dominijanni et al., 2018). The extent of solute restriction depends on the membrane efficiency coefficient, ω, which typically varies from zero for non-membranes to unity for ideal membranes that restrict solute migration completely ($0 \leq \omega \leq 1$). When $\omega > 0$, solute flux is reduced by a combination of hyperfiltration, chemico-osmotic counter advection, and restricted diffusion (Malusis et al., 2003). These processes have been captured in theoretical models for coupled solute transport (e.g., Malusis and Shackelford, 2002c; Manassero and Dominijanni, 2003; Malusis et al., 2012; Dominijanni et al., 2013), and collectively can cause appreciable reduction in solute flux depending on the magnitude of ω.

The significance of chemico-osmotic counter advection, in particular, was investigated recently by Malusis et al. (2018) based on comparison of solute transport simulations for bentonite membranes in which chemico-osmosis was either included or omitted. The results showed that solute flux reductions due solely to chemico-osmotic counter advection increase with increasing osmotic number, N_π (a dimensionless quantity representing the relative importance of chemico-osmosis to diffusion), which is a function of ion concentration and membrane properties including ω, hydraulic conductivity, k_h, and the effective salt-diffusion coefficient, D_{se}. The simulated reductions were minor (< 10 %) for $N_\pi \leq 0.3$, which encompasses the range of N_π computed for bentonite membranes based on available experimental data (Malusis and Shackelford, 2002a,b; Kang and Shackelford, 2011; Dominijanni et al., 2013; Malusis et al., 2015; Malusis and Daniyarov, 2016). However, the experimental data are limited, and higher values of N_π may be possible.

The objective of this study is to further explore the

significance of chemico-osmosis on solute migration in bentonite membranes using a phenomenological transport framework combined with a physical model relating the macroscale properties of the bentonite, namely ω and k_h, to the microscale physicochemical and fabric properties (Dominijanni and Manassero, 2005, 2012a,b; Dominijanni et al., 2017; Manassero, 2020). The model is used to simulate the coupled transport of a monovalent salt (KCl) through a sodium bentonite GCL for different source concentrations and void ratios based on predicted values of N_π.

2 PHENOMENOLOGICAL FRAMEWORK

The phenomenological framework for describing coupled fluxes of liquid and ions in clay membranes is based on principles of irreversible thermodynamics for non-equilibrium systems (Katchalsky and Curran, 1965). For a membrane in contact with a single-salt (single cation, single anion) solution, the liquid flux, q, and solute flux, J_j, may be written as follows (Malusis et al. 2012):

$$q = q_h + q_\pi = -\frac{k_h}{\gamma_w}\frac{\partial P}{\partial x} + \omega\frac{k_h}{\gamma_w}\frac{\nu}{\nu_j}RT\frac{\partial C_j}{\partial x} \quad (1a)$$

$$J_j = (1-\omega)q_h C_j + (1-\omega)q_\pi C_j - (1-\omega)nD_{se}\frac{\partial C_j}{\partial x} \quad (1b)$$

or, in dimensionless form,

$$q^* = \frac{qL}{nD_{se}} = P_e + N_\pi\frac{\partial U_j}{\partial Z} \quad (2a)$$

$$J_j^* = \frac{J_j L}{nD_{se}C_{oj}} = (1-\omega)\left[P_e U + N_\pi U\frac{\partial U}{\partial Z} - \frac{\partial U}{\partial Z}\right] \quad (2b)$$

where q_h = hydraulic liquid flux, q_π = chemico-osmotic liquid flux, γ_w = unit weight of water, P = pressure, R = universal gas constant, T = absolute temperature, ν = total number of ions per molecule of salt, ν_j = number of ions of species j per molecule of salt, C_j = concentration of species j, n = porosity, D_{se} = effective salt diffusion coefficient (= $\tau_m D_{so}$, where τ_m = matrix tortuosity factor, D_{so} = free-solution (aqueous) salt diffusion coefficient), P_e = Péclet number, U = normalized solute concentration (= C_j/C_{oj} where C_{oj} = source concentration), and Z = normalized distance (= x/L, where L = membrane thickness). The Péclet number represents the relative importance of hydraulic flow (q_h) to diffusion, whereas the osmotic number represents the relative importance of chemico-osmosis (q_π) to diffusion. These two dimensionless quantities may be expressed as follows:

$$P_e = \frac{q_h L}{nD_{se}} \quad ; \quad N_\pi = \omega\frac{\nu k_h RTC_{oj}}{\nu_j nD_{se}\gamma_w} \quad (3)$$

The terms containing N_π in Eqs. 2a,b represent the components of the liquid and solute fluxes, respectively, resulting from chemico-osmosis. Thus, the influence of chemico-osmosis can be examined by comparing solute transport simulations based on Eqs. 2a,b with the same simulations performed assuming $N_\pi = 0$. In this latter case, Eqs. 2a,b reduce to the following forms:

$$q^*(N_\pi = 0) = P_e \quad (4a)$$

$$J_j^*(N_\pi = 0) = (1-\omega)\left[P_e U - \frac{\partial U}{\partial Z}\right] \quad (4b)$$

3 PHYSICAL MODEL

The physical model provides a method for predicting ω, P_e, and N_π for bentonite membranes based on constitutive relationships for the macroscopic barrier properties as a function of physicochemical and fabric properties of the clay (montmorillonite) at the microscale. The model is based on montmorillonite fabric that is conceptualized as crystalline platelets (lamellae) organized (aggregated) as groups (tactoids) in parallel alignment (see Fig. 1). The hydrated tactoids are surrounded by adsorbed layers (diffuse double layers, or DDLs) of water and ions to balance the negative surface charge of the clay. The smaller spaces (nm) between the platelets within a tactoid (defined by the distance $2b_n$) and the spaces taken by the first row of hydrated cations in contact with the negative surfaces of the tactoids (Stern layer with thickness = d_{st}) are termed *nano-pores* and comprise the nano-pore component of the void ratio, e_n. The larger spaces (μm) between tactoids, defined by the distance $2b_m$, are termed *micro-pores* and comprise the micro-void ratio, e_m. The total void ratio, e, is the sum of these components ($e = e_m + e_n$).

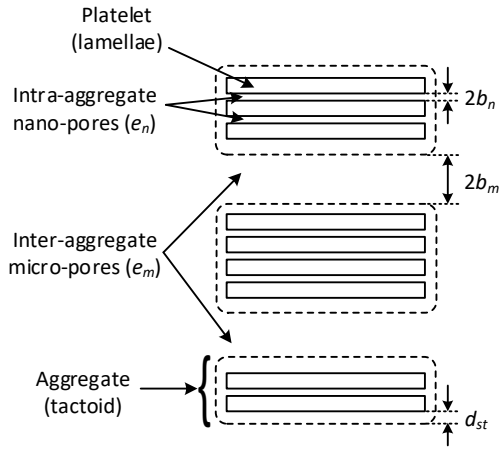

Fig. 1. Conceptual view of montmorillonite fabric showing clay platelets (lamellae) aggregated into three tactoids arranged in parallel (redrawn after Manassero, 2020; b_n = half-distance between platelets, b_m = half-distance between adjacent tactoids, d_{st} = thickness of Stern layer surrounding each tactoid).

Only the micro-pores are considered to be accessible by liquid and ions passing through the membrane. If the montmorillonite is perfectly dispersed into individual lamellae, the nano-void ratio (e_n) would comprise a larger portion of e, and the micro-pores would be smaller and more tortuous. However, tactoids will naturally form due to internal flocculation of the lamellae, reducing the surface area of the montmorillonite and increasing e_m.

Following Manassero (2020), the effective specific surface, S_{eff}, associated with the external surfaces of the tactoids is reduced relative to the maximum specific surface, S, for perfectly dispersed lamellae by the average number of lamellae per tactoid, $N_{l,AV}$, as follows:

$$S_{eff} = \frac{S}{N_{l,AV}} \tag{5}$$

Also, the nano-void ratio, e_n, is related to S_{eff} and $N_{l,AV}$ as follows:

$$e_n = b_n \rho_s \left(S_n + \frac{S \cdot d_{st}}{b_n \cdot N_{l,AV}} \right) \tag{6}$$

where $S_n = S - S_{eff}$ and ρ_s is the density of the solids. The micro-void ratio, e_m, comprises the remainder of the void ratio ($e_m = e - e_n$), with an average half-distance between tactoids, b_m, given as follows:

$$b_m = \frac{e_m}{\rho_s S_{eff}} \tag{7}$$

Thus, for a given e, larger tactoids (higher $N_{l,AV}$) yield lower S_{eff}, lower e_n, and larger, less tortuous micropores, resulting in higher k_h. Neglecting electro-viscous effects, k_h may be approximated as follows:

$$k_h = \frac{\tau_m \gamma_w e_m^3}{3\mu_w (1+e_m)(\rho_s S_{eff})^2} \tag{8}$$

where μ_w = viscosity of water.

The reduction in specific surface also reduces the effective charge concentration of the solid skeleton, $\bar{C}_{sk,0}$, as follows:

$$\bar{C}_{sk,0} = \frac{(1-f_{st})\sigma \cdot \rho_s S_{eff}}{F} \tag{9}$$

where f_{st} = fraction of surface charge compensated by the cations in the Stern layer (typically 0.7-0.95), σ = surface charge density, and F = Faraday's constant (96,490 C/mol). Lower $\bar{C}_{sk,0}$ results in less ion exclusion from the membrane pores, yielding lower ω. The expression for ω for the case of a 1:1 electrolyte is given as follows:

$$\omega = 1 - \frac{1}{\sqrt{\left(\frac{\bar{C}_{sk,0}}{2C_s e_m}\right)^2 + 1} + (2t_c - 1)\left(\frac{\bar{C}_{sk,0}}{2C_s e_m}\right)} \tag{10}$$

where

$$t_c = \frac{D_{0c}}{D_{0c} + D_{0a}} \tag{11}$$

and C_s = salt concentration, t_c = cation transport number, and D_{0c}, D_{0a} = free-solution diffusion coefficients for the cation and anion, respectively.

Based on the aforementioned equations, the magnitudes of both k_h and ω for a bentonite membrane are a function of e_m, $N_{l,AV}$, and C_s. Given a membrane with a specific total void ratio, e (which is influenced by stress history), e_m is a function of $N_{l,AV}$ by virtue of Eq. 6 and the fact that $e_m = e - e_n$. Furthermore, $N_{l,AV}$ is sensitive to the concentration of the ions in the salt solution, with higher concentrations causing more aggregation of lamellae and higher $N_{l,AV}$. Thus, prediction of k_h and ω (which is necessary to predict N_π via Eq. 3) requires knowledge of the total void ratio and the *fabric boundary surface* of the bentonite, which is the combination of e_m, $N_{l,AV}$, and C_s (Manassero, 2020).

Manassero (2020) proposed the following equations for characterizing the fabric boundary surface of bentonite exposed to monovalent salt solutions (e.g., NaCl, KCl) based on analysis of experimental data for different sodium bentonites:

$$N_{l,AV} = N_{l,AV0} + \frac{\alpha}{e_m}(C_s + 1) + \beta e_m \left[1 - \exp(-C_s)\right] \tag{12}$$

$$e_m = \frac{e \cdot N_{l,AV} - S\rho_s b_n \left[N_{l,AV} + (d_{st}/b_n) - 1\right]}{N_{l,AV}} \tag{13}$$

where $N_{l,AV0}$ = ideal average minimum number of lamellae per tactoid when $C_s = 0$ and $e_m \rightarrow \infty$, $\alpha = e_m \cdot (N_{l,AV} - N_{l,AV0})$ for $C_s = 0$, and β is a constriction coefficient accounting for mechanical constraints hindering the movement of lamellae at medium to high void ratio. These three parameters ($N_{l,AV0}$, α, β) are unique for a given bentonite, but can be estimated from laboratory tests (see Manassero, 2020). Substitution of Eq. 13 into Eq. 12 yields a cubic expression relating $N_{l,AV}$ and e for given values of $N_{l,AV0}$, α, β, S, ρ_s, b_n, and d_{st}. Once $N_{l,AV}$ is determined for a given e and C_s, Eqs. 5-11 may be used to compute k_h and ω.

4 STEADY-STATE ANALYSIS

The analysis of water and salt transport is conducted herein for the bentonite-based liner shown in Fig. 2, under steady-state conditions. The height of the ponded leachate overlying the liner is h_p. The difference in the hydraulic head across the liner is $\Delta h = (h_p + L)$, where L is the liner thickness. The void ratio, e, is assumed not to vary across the liner. Similarly, the fabric parameters (e_m, e_n, $N_{l,AV}$) are assumed to be constant across the liner and related only to the average salt concentration, $C_{avg} = (C_{s0} + C_{se})/2$, where C_{s0} is the source salt (1:1 electrolyte)

concentration in the leachate and C_{se} is the salt concentration in the layer underlying the liner. Also, $\bar{C}_{sk,0}$ and k_h depend on C_{avg}, but are constant across the liner. The only quantity that is assumed to vary across the liner is the salt concentration, C_s.

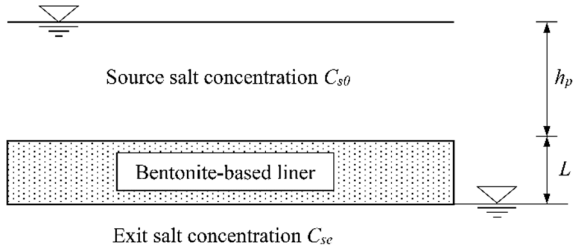

Fig. 2. Reference scenario for the steady-state analysis.

Under such conditions, the analytical solutions for the steady-state nondimensional liquid flux, q_{ss}^*, and salt flux, J_{ss}^*, are given as follows:

$$q_{ss}^* = P_e - N_{\pi g}\left(1-U_e\right) \tag{14}$$

$$J_{ss}^* = \left(1-\omega_g\right)\frac{\left[P_e - N_{\pi g}\left(1-U_e\right)\right]}{\exp\left[P_e - N_{\pi g}\left(1-U_e\right)\right]-1}\cdot \left\{\exp\left[P_e - N_{\pi g}\left(1-U_e\right)\right]-U_e\right\} \tag{15}$$

where

$$N_{\pi g} = \omega_g \frac{2k_h RTC_{s0}}{nD_{se}\gamma_w} \tag{16}$$

$$\omega_g = 1+\frac{\bar{C}_{sk,0}}{2e_m\left(C_{s0}-C_{se}\right)}\left[Z_2 - Z_1 - \left(2t_c-1\right)\ln\left(\frac{Z_2+2t_c-1}{Z_1+2t_c-1}\right)\right] \tag{17}$$

$$Z_1 = \sqrt{1+\left(2C_{s0}e_m/\bar{C}_{sk,0}\right)^2} \tag{18}$$

$$Z_2 = \sqrt{1+\left(2C_{se}e_m/\bar{C}_{sk,0}\right)^2} \tag{19}$$

$$U_e = C_{se}/C_{s0} \tag{20}$$

In these equations, the subscript "g" in $N_{\pi g}$ and ω_g stands for the "global" value, which represents an average quantity over the liner thickness (Dominijanni et al., 2018). Note that, for a 1:1 electrolyte, N_π in Eq. 3 is equivalent to $N_{\pi g}$ in Eq. 16.

5 OSMOTIC NUMBER PREDICTION

In this paper, global osmotic numbers, $N_{\pi g}$, are predicted for a GCL containing sodium bentonite. The total specific surface, S, surface charge density, σ, and solids density, ρ_s, are assumed to be 750 m^2/g, 0.114 C/m^2, and 2.61 Mg/m^3, respectively (Petrov et al. 1997; Manassero, 2020). The Stern layer thickness, d_{st}, the half-distance between lamellae in a tactoid, b_n, and the Stern fraction, f_{st}, are expected to lie within the relatively narrow ranges of 1.2-2.0 nm, 0.2-0.5 nm, and 0.70-0.95, respectively (Laird, 2006; Dominijanni et al., 2017; Manassero, 2020). For this study, d_{st} = 1.8 nm, b_n = 0.45 nm, and f_{st} = 0.90 are assumed. Also, the temperature is 293 K (20 °C) and the solution viscosity and unit weight are $1.0\text{x}10^{-3}$ Pa·s and 9.81 kN/m^3, respectively.

For the fabric boundary surface, the parameters $N_{l,AV0}$, α, and β in Eq. 12 are estimated as 2.85, 8.49, and 9.39, respectively, based on calibration with experimental data reported for GCLs by Petrov and Rowe (1997) and Malusis and Shackelford (2002a). Petrov and Rowe (1997) measured k_h for a GCL (e = 1.60-4.89) permeated with different NaCl solutions (C_{s0} = 10-2000 mM), whereas Malusis and Shackelford (2002a) measured ω_g for a GCL (e = 2.85-6.14) with different KCl solutions (C_{s0} = 3.9-47 mM). Although the GCLs and the salt type differed in these two studies, a single fabric boundary surface defined by $N_{l,AV0}$ = 2.85, α = 8.49, and β = 9.39 provides reasonably good fits to both the k_h and ω_g data sets, as shown in Fig. 3.

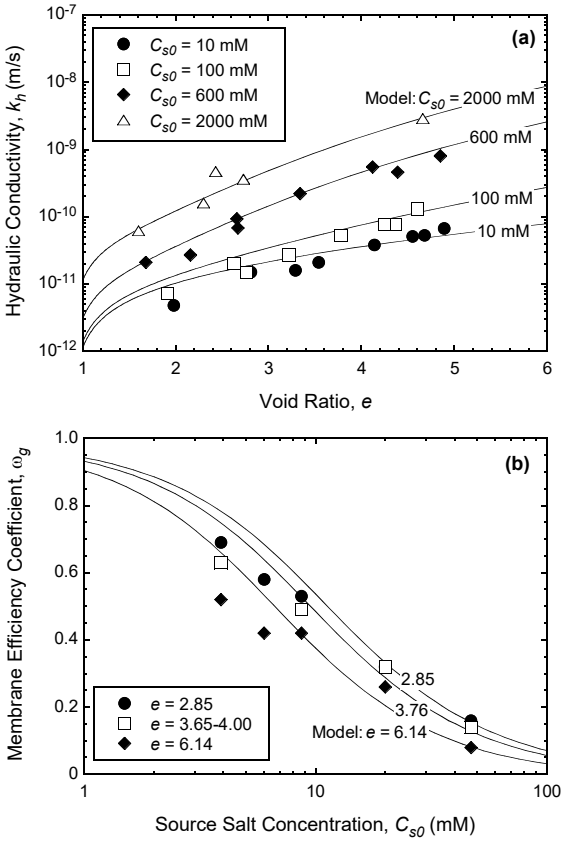

Fig. 3. Comparison of experimental data and model predictions for sodium bentonite GCLs based on fabric boundary surface parameters $N_{l,AV0}$ = 2.85, α = 8.49, and β = 9.39: (a) hydraulic conductivity to NaCl solutions (Petrov and Rowe, 1997); (b) global membrane efficiency coefficients for KCl solutions (Malusis and Shackelford, 2002a).

Given the aforementioned set of physicochemical and fabric parameters, predicted values of k_h, ω_g, and $N_{\pi g}$ were determined for a representative sodium bentonite GCL subjected to KCl solutions (D_{so} = 19.93x10^{-10} m^2/s, t_c = 0.491) for source salt concentrations, C_{s0}, ranging from 1-1000 mM. For determination of ω_g and $N_{\pi g}$ via Eqs. 16-19, the exit salt concentration, C_{se}, is assumed to be zero (i.e., a perfectly-flushing exit boundary condition), such that the average salt concentration is $C_{avg} = C_{s0}/2$. Two different void ratios are considered: (1) e = 4.0, representing a GCL subjected to a relatively low effective confining stress (~35 kPa); and (2) e = 2.0, representing a GCL subjected to a relatively high effective confining stress (~240 kPa) (see Kang and Shackelford, 2010). The matrix tortuosity factors are estimated based on Malusis et al. (2015) as τ_m = 0.14 for e = 4.0 and τ_m = 0.08 for e = 2.0.

The predicted values of k_h and ω_g are plotted as a function of C_{s0} in Fig. 4. For a given C_{s0}, lower k_h and higher ω_g are predicted for the GCL with the lower void ratio (e = 2.0) relative to the GCL with the higher void ratio (e = 4.0), as expected, given the lower τ_m and lower micro-void ratio (e_m) associated with e = 2.0. For a given e, k_h increases and ω_g decreases with increasing C_{s0}, since higher C_{s0} causes more aggregation of lamellae (higher N_{LAV}), yielding higher e_m and lower $\bar{C}_{sk,0}$.

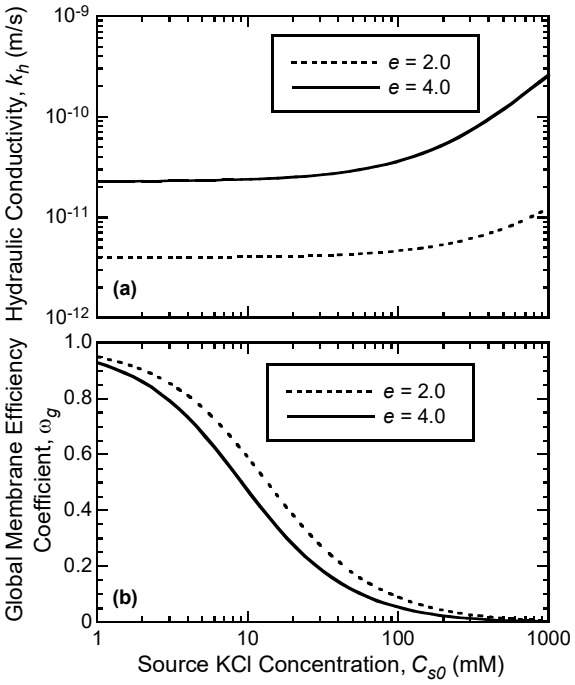

Fig. 4. Predictions of (a) k_h and (b) ω_g for GCL at low void ratio (e = 2.0) and high void ratio (e = 4.0) as a function of source KCl concentration.

Although k_h is relatively insensitive to salt concentration at low C_{s0} (Fig. 4a), increases in k_h become more significant as C_{s0} increases beyond 100 mM due to substantially greater aggregation of lamellae. As a result, ω_g is substantially reduced but remains slightly greater than zero, even at C_{s0} = 1,000 mM (Fig. 4b). Low, but non-zero, predicted values of ω_g at C_{s0} > 100 mM are consistent with the experimental results of Shackelford et al. (2016), who reported ω_g = 0.006 for a GCL with C_{s0} = 200 mM KCl. Also, Sherwood and Craster (2000) reported ω_g = 0.0011 for a sodium bentonite specimen tested using C_{s0} = 3,500 mM KCl. For the fabric boundary surface parameters employed in this study, the model overpredicts ω_g at C_{s0} = 200 mM relative to the ω_g reported by Shackelford et al. (2016) (i.e., ω_g = 0.023 relative to ω_g = 0.006). Nonetheless, the model supports these and other experimental observations (e.g., Meier et al., 2014) that membrane behavior may persist even at very high source concentrations.

Despite the trend of decreasing ω_g with increasing C_{s0} (Fig. 4b), predicted values of the global osmotic number, $N_{\pi g}$, increase with increasing C_{s0}, as illustrated in Fig. 5. Based on Eq. 16, $N_{\pi g}$ is directly proportional to not only ω_g but also C_{s0} and k_h, which increases with C_{s0} (see Fig. 4a). The competing influences of ω_g, C_{s0}, and k_h limit the magnitude of predicted $N_{\pi g}$ to ≤ 0.3 for e = 2.0 over the full range of source concentrations considered. For e = 4.0, $N_{\pi g}$ is predicted to be ≤ 0.3 for C_{s0} ≤ 20 mM.

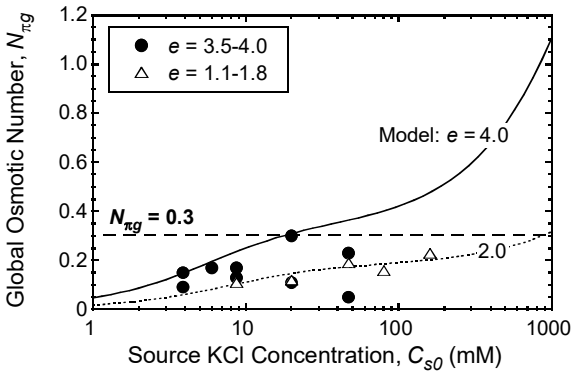

Fig. 5. Comparison of predicted values of $N_{\pi g}$ from the model in this study with experimentally derived values of $N_{\pi g}$ reported by Malusis et al. (2018) for GCLs with KCl solutions.

As noted by Malusis et al. (2018), limited experimental studies have been conducted on GCLs in which all parameters needed to quantify $N_{\pi g}$ were measured and reported (Malusis and Shackelford, 2002a,b; Kang and Shackelford, 2011; Dominijanni et al., 2013; Malusis et al., 2015; Malusis and Daniyarov, 2016). Values of $N_{\pi g}$ computed by Malusis et al. (2018) based on experimental data generated for GCLs using KCl solutions are compared with the predicted $N_{\pi g}$ curves for e = 2.0 and e = 4.0 in Fig. 5. The results illustrate that the predictions are reasonably consistent with the experimental observations. All of the

experimental $N_{\pi g}$ values are ≤ 0.3, and $N_{\pi g}$ values for the specimens with lower void ratios (e = 1.1 to 1.8) are similar to the predicted $N_{\pi g}$ for e = 2.0. The specimens with higher void ratios (e = 3.5 to 4.0) exhibit more scatter, but all of the $N_{\pi g}$ values plot either on or below the predicted $N_{\pi g}$ curve for e = 4.0.

The predicted $N_{\pi g}$ curve for e = 4.0 in Fig. 5 increases more sharply as C_{s0} increases beyond ~100 mM due to the more sharply increasing k_h at these higher concentrations (see Fig. 4a), suggesting that $N_{\pi g}$ values substantially higher than 0.3 are possible. However, no experimental data are present in Fig. 5 for C_{s0} > 50 mM and e = 3.5-4.0, as no studies have yet been conducted on GCLs at these higher void ratios in which all parameters needed to compute $N_{\pi g}$ have been measured for KCl solutions.

6 INFLUENCE OF CHEMICO-OSMOSIS

The aforementioned analyses of steady-state water and salt (KCl) transport through the bentonite-based liner in Fig. 2 (see Section 4) were performed based on the model results for k_h, ω_g, and $N_{\pi g}$ in Figs. 4 and 5, assuming a perfectly-flushing lower boundary condition (C_{se} = 0). The height of the ponded leachate, h_p, is assumed to be 300 mm (~1 ft), the maximum allowable ponding height for a landfill in the US. The barrier thickness is assumed to be 10 mm (representing a typical GCL), yielding a hydraulic gradient, $i = (h_p+L)/L$ = 31, assuming zero suction at the GCL foundation interface. The resulting Péclet numbers, P_e, based on Eq. 3 (where $q_h = k_h i/n$) are plotted as a function of C_{s0} in Fig. 6. Note that P_e is not constant for a given e, but rather increases with C_{s0} in a similar manner as k_h (Fig. 4a).

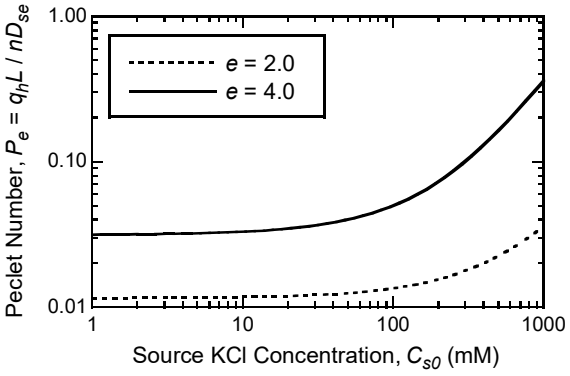

Fig. 6. Péclet numbers for steady-state analysis of liquid and salt (KCl) transport as a function of source concentration.

Values of the steady-state liquid flux, q_{ss}^*, and salt flux, J_{ss}^*, given by Eqs. 14 and 15 are plotted as a function of C_{s0} in Fig. 7. If chemico-osmosis is neglected ($N_{\pi g}$ = 0), Eqs. 14 and 15 reduce to the following forms (given C_{se} = 0):

$$q_{ss}^*\left(N_{\pi g}=0\right)=P_e \tag{21}$$

$$J_{ss}^*\left(N_{\pi g}=0\right)=\left(1-\omega_g\right)P_e\frac{\exp\left(P_e\right)}{\exp\left(P_e\right)-1} \tag{22}$$

Although $N_{\pi g}$ = 0 is not compatible with $\omega_g \neq 0$ (see Eq. 16), Eq. 22 allows the contributions of hyperfiltration and restricted diffusion to be included in the salt flux.

If membrane behavior is neglected altogether (i.e., ω_g = 0), the liquid flux remains unchanged from Eq. 21, but Eq. 22 reduces to the following expression:

$$J_{ss}^*\left(\omega_g=0\right)=P_e\frac{\exp\left(P_e\right)}{\exp\left(P_e\right)-1} \tag{23}$$

Thus, neglecting chemico-osmosis by assuming $N_{\pi g}$ = 0 yields the same liquid flux as neglecting membrane behavior entirely, whereas the salt flux is still influenced by ω_g (i.e., due to hyperfiltration and restricted diffusion) even if chemico-osmosis is ignored. The predicted liquid and salt flux curves for the case of $N_{\pi g}$ = 0 and the predicted salt flux curves for the case of ω_g = 0 also are shown in Fig. 7 for comparison. Note that the curves for liquid flux when $N_{\pi g}$ = 0 are the same as the P_e curves in Fig. 6, since $q_{ss}^* = P_e$ when $N_{\pi g}$ = 0 (see Eq. 21).

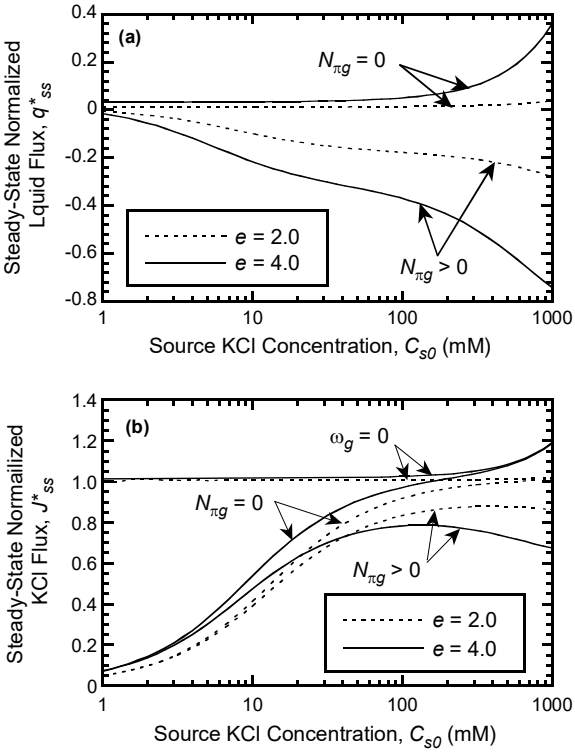

Fig. 7. Predictions of (a) steady-state normalized liquid flux, q_{ss}^*, and (b) steady-state normalized salt (KCl) flux, J_{ss}^*, as a function of source concentration and void ratio.

The results in Fig. 7a indicate that, when chemico-osmosis is included in the model simulations, the net liquid flux through the barrier is upward (negative), since $N_{\pi g} > P_e$ over the entire range of C_{s0} considered. Furthermore, the magnitude of q^*_{ss} increases with increasing C_{s0}, because $N_{\pi g}$ increases with C_{s0} (Fig. 5). In contrast, the liquid fluxes are downward (positive) when chemico-osmosis is ignored, since the hydraulic component of the liquid flux is downward (see Fig. 2).

For salt flux, the results in Fig. 7b show that, for a given e, ignoring chemico-osmosis by assuming $N_{\pi g} = 0$ results in overprediction of J^*_{ss}, as expected (e.g., Malusis and Shackelford 2004). As the source concentration, C_{s0}, approaches 1,000 mM, the J^*_{ss} curves for the case of $N_{\pi g} = 0$ approach the limiting values of J^*_{ss} for the case in which membrane behavior is ignored entirely ($\omega_g = 0$), since ω_g approaches zero as C_{s0} approaches 1,000 mM (Fig. 4b).

Interestingly, the model predicts higher salt fluxes for the lower void ratio ($e = 2.0$) relative to the higher void ratio ($e = 4.0$) for $C_{s0} \geq 50$ mM when chemico-osmosis is included in the analysis. This counter-intuitive result is apparently due to the sharp increase in $N_{\pi g}$ for $e = 4.0$ beyond $C_{s0} = 50$ mM (Fig. 5), which yields a sharp increase in the upward liquid flux (Fig. 7a). However, given that the predicted $N_{\pi g}$ curve for $e = 4.0$ and $C_{s0} > 50$ mM in Fig. 5 is not supported by measured data, more experiments are needed to validate the model predictions.

The percent errors in salt flux caused by ignoring chemico-osmosis are illustrated in Fig. 8a. The errors range from 1-20 % for $e = 2.0$ at all source concentrations and for $e = 4.0$ at lower source concentrations ($C_{s0} < 50$ mM). Greater errors are predicted (i.e., 20-80 %) for $e = 4.0$ at $C_{s0} = 50$-1,000 mM. These errors are modest in comparison to the errors caused by neglecting membrane behavior entirely, which can exceed 1,000 % at low C_{s0} (see Fig. 8b). Nonetheless, the errors are easily avoided by using a complete coupled flux framework (e.g., Eqs. 1a,b) for modeling solute transport though a GCL when membrane behavior exists.

6 CONCLUSIONS

The results of this study illustrate the use of a combined phenomenological (macro-scale) and physical (micro-scale) model to predict coupled electrolyte (salt) transport through a bentonite barrier (GCL). The physical model was used to predict the global membrane efficiency coefficient, ω_g, hydraulic conductivity, k_h, Péclet number, P_e, and global osmotic number, $N_{\pi g}$, for a representative GCL as a function of the source salt (KCl) concentration based on a calibrated fabric boundary surface for the bentonite. The predicted $N_{\pi g}$ values from the physical model were reasonably consistent with $N_{\pi g}$ values computed from limited experimental data for GCLs, which were ≤ 0.3 in all cases. The physical model predicts that $N_{\pi g}$ increases with increasing source KCl concentration (despite a decrease in ω_g) and that $N_{\pi g} > 0.3$ is possible for a GCL at lower confining stresses (higher void ratios) subjected to source KCl concentrations exceeding 50 mM. However, more experimental data are needed to validate the model predictions at higher source concentrations.

The predicted P_e and $N_{\pi g}$ were incorporated into a phenomenological solute transport model to assess the influence of chemico-osmosis on liquid and salt flux under steady-state conditions. The model results showed that chemico-osmosis becomes increasingly more significant with increasing source KCl concentration (due to increasing $N_{\pi g}$), such that appreciable errors can be inherent in salt flux predictions if the influence of chemico-osmosis is neglected.

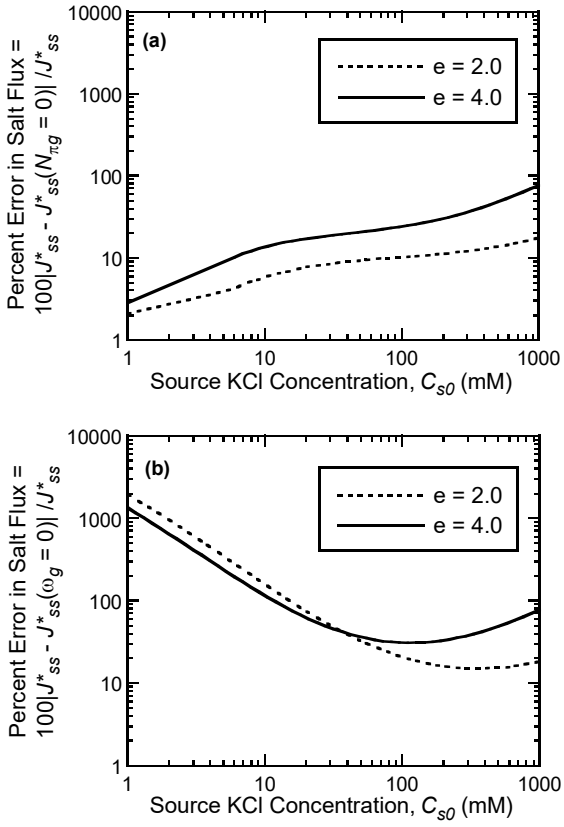

Fig. 8. Percent errors in predicted steady-state salt flux caused by (a) ignoring chemico-osmosis ($N_{\pi g} = 0$), and (b) ignoring membrane behavior entirely ($\omega_g = 0$).

REFERENCES

1) Bohnhoff, G. and Shackelford, C. (2013): Improving membrane performance via bentonite polymer nanocomposite. *Applied Clay Science,* 86, 83-98.
2) Dominijanni, A. and Manassero, M. (2005): Modelling osmosis and solute transport through clay membrane barriers. In: *Proceedings of Geo-Frontiers 2005*, Geotechnical Special

Publication (GSP) 130-142, ASCE, Reston, VA, 3437-3448.
3) Dominijanni, A. and Manassero, M. (2012a): Modelling the swelling and osmotic properties of clay soils. Part I: The phenomenological approach. *International Journal of Engineering Science*, 51, 32-50.
4) Dominijanni, A. and Manassero, M. (2012b): Modelling the swelling and osmotic properties of clay soils. Part II: The physical approach. *International Journal of Engineering Science*, 51, 51-73.
5) Dominijanni, A., Guarena, N. and Manassero, M. (2018): Laboratory assessment of semi-permeable properties of a natural sodium bentonite. *Canadian Geotechnical Journal*, 55(11), 1611-1631.
6) Dominijanni, A., Manassero, M., Boffa, G. and Puma, S. (2017): Intrinsic and state parameters governing the efficiency of bentonite barriers for contaminant control. In: *Proceedings of the International Workshop on Advances in Laboratory Testing and Modelling of Soils and Shales*, Ferrari, A. and Laloui, L., Eds., Springer International Publishing, Cham, Switzerland, 45-56.
7) Dominijanni, A., Manassero, M. and Puma, S. (2013): Coupled chemical-hydraulic-mechanical behaviour of bentonites. *Géotechnique*, 63(3), 191-205.
8) Kang, J. and Shackelford, C. (2010): Consolidation of a geosynthetic clay liner under isotropic states of stress. *Journal of Geotechnical and Geoenvironmental Engineering*, 136(1), 253-259.
9) Kang, J. and Shackelford, C. (2011): Consolidation enhanced membrane behavior of a geosynthetic clay liner. *Geotextiles and Geomembranes,* 29, 544- 556.
10) Katchalsky, A., Curran, P. (1965): *Nonequilibrium Thermodynamics in Biophysics*. Harvard University Press, Cambridge, Mass.
11) Laird, D. (2006): Influence of layer charge on swelling of smectites. *Applied Clay Science*, 34(1-4), 74–87.
12) Malusis, M. and Daniyarov, A. (2016): Membrane efficiency and diffusive tortuosity of a dense prehydrated geosynthetic clay liner. *Geotextiles and Geomembranes,* 44, 719-730.
13) Malusis, M. and Shackelford, C. (2002a): Chemico- osmotic efficiency of a geosynthetic clay liner. *Journal of Geotechnical and Geoenvironmental Engineering,* 128, 97-106.
14) Malusis, M. and Shackelford, C. (2002b): Coupling effects during steady-state solute diffusion through a semipermeable clay membrane. *Environmental Science and Technology,* 36, 1312-1319.
15) Malusis, M. and Shackelford, C. (2002c): Theory for reactive solute transport through clay membrane barriers. *Journal of Contaminant Hydrology,* 59, 291-316.
16) Malusis, M. and Shackelford, C. (2004): Predicting solute flux through a clay membrane barrier. *Journal of Geotechnical and Geoenvironmental Engineering*, 130(5), 477-487.
17) Malusis, M., Kang, J., and Shackelford, C. (2015): Restricted solute diffusion in a geosynthetic clay liner. *Environmental Geotechnics,* 2(2), 68-77.
18) Malusis, M., Scalia, J., Norris, A., and Shackelford, C. (2018). Effect of chemico-osmosis on solute transport in clay barriers. *Environmental Geotechnics*, online ahead of print, 1-10. https://doi.org/10.1680/jenge.17.00109.
19) Malusis, M., Shackelford, C., and Maneval J. (2012): Critical review of coupled flux formulations for clay membranes based on nonequilibrium thermo- dynamics. *Journal of Contaminant Hydrology,* 138-139, 40-59.
20) Malusis, M., Shackelford, C., and Olsen, H. (2003): Flow and transport through clay membrane barriers. *Engineering Geology,* 70(2-3), 235-248.
21) Manassero, M. (2020): Second ISSMGE R. Kerry Rowe Lecture: On the intrinsic, state, and fabric parameters of active clays for contaminant control. *Canadian Geotechnical Journal*, 57(3), 311-336.
22) Manassero, M. and Dominijanni, A. (2003): Modelling the osmosis effect on solute migration through porous media. *Géotechnique*, 53(5), 481-492.
23) Mazzieri, F., Van Impe, P., and Di Emidio, G. (2005): Chemico-osmotic behaviour of modified "multi- swellable" bentonite. In: *Proceedings of the 16th International Conference on Soil Mechanics and Geotechnical Engineering,* Millpress, Rotterdam, 2297-2300.
24) Mazzieri, F., Van Impe, P., Van Impe, W., and Constales, D. (2003): Measurement of chemico-osmotic parameters of clayey soils. In: *Proceedings of the 13th European Conference on Soil Mechanics and Geotechnical Engineering,* Balkema, Rotterdam, 433-438.
25) Meier, A., Sample-Lord, K., Castelbaum, D., Kallase, S., Moran, B., Ray, T., and Shackelford, C. (2014): Persistence of semipermeable membrane behavior for a geosynthetic clay liner. In: *Proceedings, 7th International Conference on Environmental Geotechnics*, A. Bouazza, S. Yuen, and B. Brown, Eds., Engineers Australia, Barton, Australia, 496-503.
26) Petrov, R., and Rowe, R. (1997): Geosynthetic clay liner (GCL) – chemical compatibility by hydraulic conductivity testing and factors impacting its performance, *Canadian Geotechnical Journal*, 34(6), 863–885.
27) Petrov, R., Rowe, R., Quigley, R. (1997): Selected factors influencing GCL hydraulic conductivity. *Journal of Geotechnical and Geoenvironmental Engineering*, 123(8), 683-695.
28) Shackelford, C., Meier, A., Sample-Lord, K. (2016): Limiting membrane and diffusion behavior of a geosynthetic clay liner. *Geotextiles and Geomembranes,* 44, 707-718.
29) Shackelford, C. and Scalia, J. (2016): Semipermeable membrane behaviour in bentonite-based barriers: past, present, and future. In: *GeoVancouver 2016*, Canadian Geotechnical Society, Richmond, BC, Canada, paper 4173.
30) Sherwood, J. and Craster, B. (2000): Transport of water and ions through a clay membrane. *Journal of Colloid and Interface Science*, 230, 349-358.